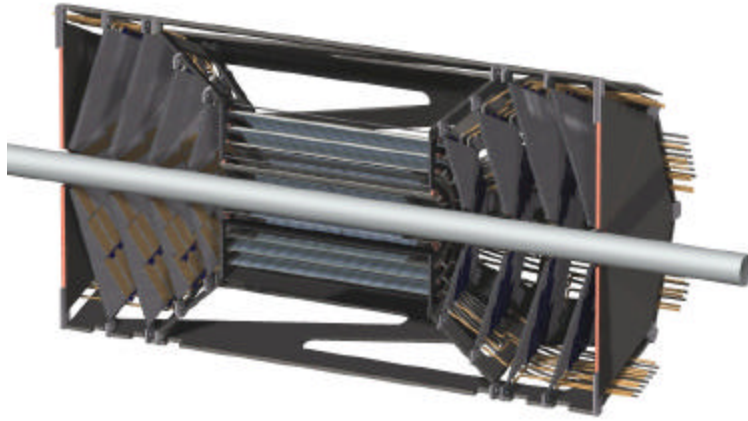


# Silicon Vertex Upgrade for PHENIX

March 2003

V. Ciancolo, A. Drees, H. Enyo, Y. Goto, N. Grau, J. Haggerty, J. Heuser, J. Hill, G. Kunde, J. Lajoie, D. Lee, P. McGaughey, C.A. Ogilvie, H. Ohnishi, H. Pei, J. Rak, K. Read, V. Rykov, N. Saito, K. Tanida, M. Togawa, G. Tuttle, H. Van Hecke, S. White, C. Woody



<b>1. INTRODUCTION .....</b>	<b>3</b>
<b>2. GOALS OF THE SILICON VERTEX UPGRADE .....</b>	<b>4</b>
2.1 SPIN STRUCTURE OF NUCLEON .....	4
2.2 EXPLORATION OF THE NUCLEON STRUCTURE IN NUCLEI.....	6
2.3 PROBES OF EARLY, HIGHEST ENERGY-DENSITY STAGE OF HEAVY-ION REACTIONS.....	6
2.3.1 ENERGY-LOSS OF HEAVY-QUARKS .....	7
2.3.2 OPEN CHARM AND BEAUTY ENHANCEMENT .....	7
2.3.3 $J/\psi$ SUPPRESSION .....	7
2.3.4 OTHER PHYSICS TOPICS .....	7
<b>3 SIMULATIONS AND REQUIRED PERFORMANCE .....</b>	<b>8</b>
3.1 OPEN CHARM MEASUREMENT .....	9
3.2 OPEN BEAUTY MEASUREMENTS .....	12
3.3 TRIGGER PLANS .....	14
3.4 EVENT RATES .....	15
3.5 MATCHING TO SPECTROMETERS .....	15
3.6 INTEGRATION WITH PHENIX.....	15
<b>4 TECHNICAL ASPECTS OF THE PROPOSED VERTEX DETECTOR .....</b>	<b>16</b>
4.1 HYBRID PIXELS, FIRST BARREL LAYER.....	16
4.2 SILICON STRIPS .....	18
4.3 ENDCAP HYBRID PIXELS.....	20
4.4 CHANNEL COUNT .....	20
4.5 MECHANICAL STRUCTURE AND COOLING.....	20
<b>5 SCHEDULE AND RESPONSIBILITIES.....</b>	<b>22</b>
<b>6 BUDGET.....</b>	<b>24</b>

# 1. Introduction

This Letter-of-Intent outlines our plans to propose and construct a silicon vertex detector for PHENIX. We outline the physics case, specify the requirements, list possible technical options, and define the needed R&D. There are three broad areas of new physics that are made possible by the proposed Si vertex detector.

- a large increase in the range of  $x$  over which we can extract the gluon spin structure function in protons with measurements of open charm and beauty in polarized p+p reactions
- robust measurements of the shadowing of the gluon structure function in nuclei with measurements of open charm and beauty in p+A reactions
- probing the early, highest energy-density phase of the matter formed in a heavy-ion reaction using the production of heavy flavor. There are several opportunities.
  - measuring the high-pt spectra of open charm and beauty above 4 GeV/c. The energy-loss of high-pt heavy-quarks is predicted to be less than for lighter-quarks.
  - measuring the yields of both open-charm and beauty in multiple channels to firmly establish whether heavy-quarks are enhanced in the pre-equilibrium phase
  - using the open charm yield to form the ratio  $J/\psi$ /(open charm) and hence to quantify the suppression of  $J/\psi$
  - yield of epsilon states

Our physics goals require that we measure charm and beauty mesons over a broad range of rapidity and transverse momentum. The proposed vertex detector achieves this by measuring displaced tracks that are matched to the central and muon arms of PHENIX. The broad pt, y range is achieved by using different decay channels to reach different parts of phase space.

The planned upgrade will operate well at 40x design luminosity and many of the measurements need the higher luminosity, e.g. epsilon, open beauty.

The proposed detector (VTX) is shown schematically in Figure 1, where there are two distinct parts, central barrel and two endcaps. The barrel consists of four concentric layers, the first populated by Si pixel sensors, the outer three by Si strip detectors. The barrel covers  $-1.2 < \eta < 1.2$  and almost  $2\pi$  in azimuth and provides a single-track DCA resolution of  $\sim 50 \mu\text{m}$  at the vertex. The forward silicon detectors are designed to provide coverage in the angular acceptance of the forward Muon Arms. The forward silicon cover  $1.2 < |\Delta\eta| < 2.7$  and the almost full azimuth angle with a resolution of  $\sim 150 \mu\text{m}$ . Each endcap comprises four octagonal ‘‘lampshades’’ populated with Si pixel detectors..

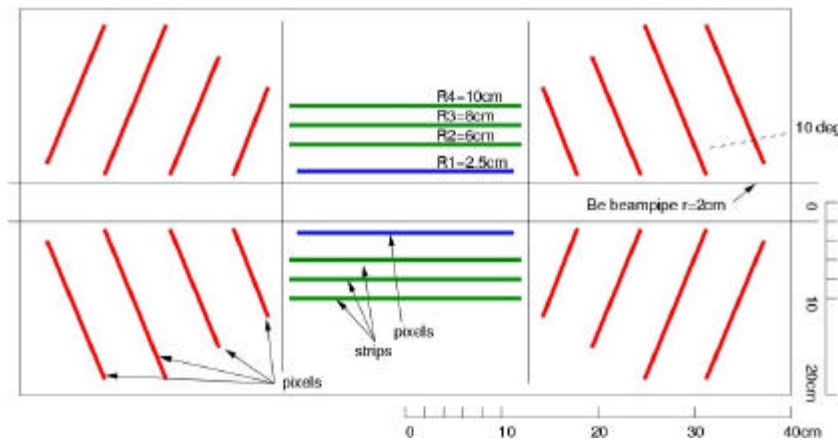


Figure 1. Cross-section view of the proposed vertex detector.

A schematic mechanical drawing developed by Hytec engineering is shown in Figure 2.

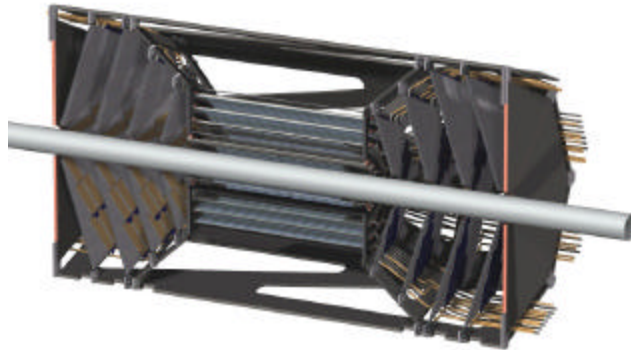


Figure 2 A schematic cut-away mechanical drawing of the proposed vertex detector (from Hytec).

The proposed detector complements the existing central and muon arm detectors and these baseline detectors are essential for the proposed physics program. Because of the different requirements to augment central tracking and muon VTX naturally separates into two projects. The barrel layers use largely existing technology and are in part funded by RIKEN. The endcaps require more R&D as described in Section 4. Hence the current plan is to stage the implementation of the VTX, first the barrel then the endcaps.

In Section 2 we provide more details on the main physics goals of the planned detector upgrade and in Section 3 we discuss the simulated performance of the detector. The specific detector components and R&D needs are discussed in Section 4, in Section 5 we discuss the schedule and institution responsibilities, and we close in Section 6 with construction costs.

## 2. Goals of the Silicon Vertex Upgrade

### 2.1 Spin Structure of Nucleon

The measured quark spin-structure function in the proton integrates to less than the required spin-1/2, a result that is described as the "spin-crisis"<sup>1</sup>. One leading possibility is that gluons carry the missing spin and as such PHENIX has a major goal of measuring the gluon spin-structure function in protons. PHENIX has existing capability shown in Figure 3 as blue lines. The different channels include direct-photons approximately back-to-back with a high-pt hadron, charm and beauty production. However there are significant gaps in this x-range that will make it difficult to fully address the spin-crisis. The proposed Si vertex detector extends the coverage to  $0.004 < x < 0.3$  as well as providing significant regions where multiple channels overlap. This overlap will provide vital cross-checks that will improve the reliability of global fits to the spin structure function.

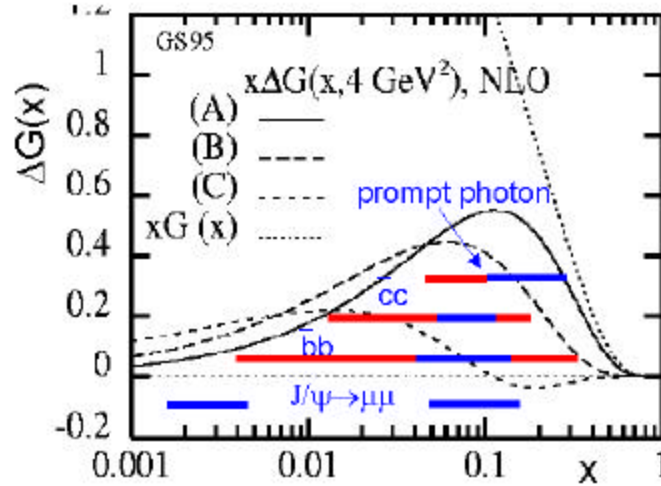


Figure 3 Expected x-range for different channels over which PHENIX will be able to extract the gluon spin structure function. The blue bars indicate PHENIX's existing capability while the red bars indicate the additional coverage provided by the proposed vertex upgrade.

The vertex detector provides the following improvements in x-range

- c c production via gluon fusion. The lower x-range is extended by identifying low pt ( $p_t > 0.5$  GeV) electrons as coming from displaced vertices from charm decay. The upgrade extends the upper x-range using  $D \rightarrow K\pi$  decay channel for high-pt D's. The existing range in x for charm is made much more robust by the addition of a detached vertex signature
- b b production via gluon fusion. With the upgrade we can identify displaced  $J/\psi$  from  $B \rightarrow J/\psi$  decay which provides coverage in x between 0.005-0.01 and 0.1-0.2. The selection of semi-leptonic decays  $b \rightarrow e\mu X$  at high momentum is clean using displaced vertices. This extends the  $x_{\text{gluon}}$  coverage for these semi-leptonic decays to 0.02-0.3.
- direct photon: The vertex detector provides the angle of the jet in coincidence with the direct photon. This constrains the x of the gluon by reconstructing its kinematics and permits lowering the range of  $p_{T}$  of the photon down to  $p_t > 5$  GeV. This extends the x coverage to 0.05 - 0.3

A third class of distributions, transversity  $\delta q(x)$  is needed for a complete description of nucleon structure at leading twist. Transversity distributions are experimentally unknown and offer a new window on nucleon spin structure with distinct advantages: Transversity involves a helicity spin flip amplitude and therefore is free of admixtures from gluons. The first moment of transversity distributions is a tensor charge and thus strictly a valence quark. The measurement of transversity distributions through spin-dependent fragmentation of hadrons requires the knowledge of the jet-axis. For example, in Collins-Heppelman fragmentation the sensitivity to the transverse quark spin results from the azimuthal distribution of hadrons around the jet-axis. The present geometric acceptance ( $\Delta\eta < 0.7$ ) of the PHENIX central arms is too small to permit a sufficient reconstruction of the jets-axis, since jets typically extend over about one unit in pseudo-rapidity. However, a new tracking device close to the interaction region would extend the geometric acceptance ( $\Delta\eta < 2.0$ ) and provide the necessary reconstruction of the jet-angle. One option may be to calculate the jet-angle from the centroid of tracks within a cone.

Before using open charm and beauty for spin asymmetry measurements we need to test the next-to-leading-order (NLO) pQCD calculations for heavy-quark production<sup>2,3</sup>. Previous comparisons have emphasized the total heavy-quark yield<sup>2</sup> in proton-proton reactions, but more stringent tests are possible with the  $p_t$  spectra<sup>4</sup>. Qualitatively, low- $p_t$  charm and beauty production are dominated by gluon-fusion, while production at high- $p_t$  is expected to be dominated by the hard-scattered gluon splitting into a  $Q\bar{Q}$  pair<sup>5</sup>.

Present data on charm and bottom production is scarce and of limited statistics and there are no charm measurements at energies above ISR energy.

## 2.2 Exploration of the nucleon structure in nuclei

Proton-nucleus collisions not only provide important key baseline information for the study of QCD at high temperatures, they also address the fundamental issues of the parton structure of nuclei. Since the discovery of the EMC effect in the 1980's, it is clear that the parton structure of a nucleon changes if it is bound in a nucleus<sup>6</sup>. One of the prime objectives for PHENIX is to measure the gluon and antiquark distributions in nuclei.

In general all processes suitable to measure the spin gluon structure in nucleons are also ideal for probing gluon distribution in nuclei. The reach in x-range is indicated in Figure-3 superimposed on calculations of the ratio of nuclear to nucleon gluon structure function<sup>7</sup>.

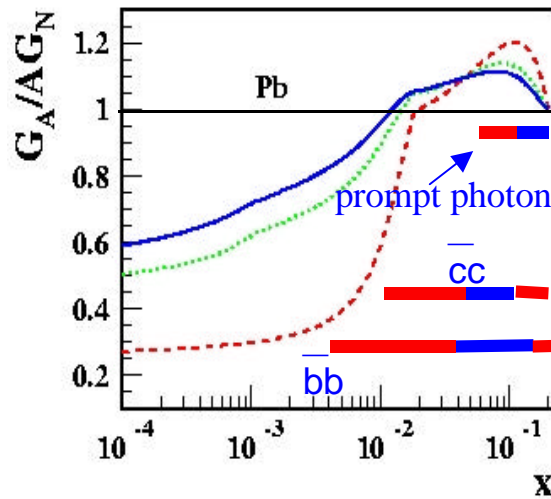


Figure 3 Gluon shadowing predictions along with PHENIX coverage. The red bars indicate the addition range provided by the vertex upgrade, while the blue bars cover the PHENIX baseline. The three theoretical predictions are for different Q transferred, blue, green and red lines are  $Q= 10, 5$  and  $2 \text{ GeV}/c$  respectively. From L. Frankfurt, M. Strikman<sup>7</sup>

The red bars indicate the additional coverage provided by the vertex upgrade compared to the baseline of PHENIX. The vertex upgrade provides extends the x-range from the anti-shadowing region into the shadowing domain which means we will be able to establish the shape of the gluon structure function. The overall normalization will require a careful cross-calibration between p+p and dAu running periods to monitor the relative luminosity.

## 2.3 Probes of Early, Highest Energy-Density Stage of Heavy-ion Reactions

As RHIC moves to the second half of this decade the focus will shift from the discovery phase to a detailed exploration of quark matter. Charm and Bottom production are key observables for the earliest, highest energy-density stage of Au+Au collisions. The information that the yield and spectra of heavy-flavor mesons will provide on the earliest stages of a collision at RHIC is discussed in the following sub-sections. Critical will be the broad reach in rapidity and transverse momentum made possible by the proposed upgrade. This extends PHENIX's existing capability of low-pt open charm.

### 2.3.1 Energy-loss of heavy-quarks

Colored high-pt partons are predicted to lose energy as they propagate through the medium<sup>8</sup>. The dominant mechanism is calculated to be medium-induced gluon radiation<sup>9,10</sup> with a smaller contribution from elastic collisions with lower-energy partons<sup>8</sup>. Heavy-quarks are predicted<sup>11</sup> to lose less energy in the plasma because of stronger destructive interference effects. Qualitatively the heavier quark is less deflected during gluon Bremsstrahlung which leads to more destructive interference in a “dead-cone” around the heavy-quark’s trajectory. To explore this physics will require measuring the pt spectra for open charm and beauty out to several GeV/c. The most promising avenue for high momenta D’s are the hadronic decay channels, e.g.  $D \Rightarrow K + \pi$  since for these momenta electrons from charm decay are dominated by electrons from B-decay.

### 2.3.2 Open Charm and Beauty Enhancement

Open charm enhancement has been predicted in the earliest stages of A+A reactions<sup>12,13,14</sup>. Heavy-quarks are produced in the initial parton-parton collisions that occur during a heavy-ion reaction and possibly also via gluon fusion in the pre-equilibrium stage of the reaction. This is the mechanism originally proposed for strangeness enhancement, but may be more powerful in the case of charm since the rate of heavy-quark production is expected to be negligible later in the reaction when the energy density has decreased. This enhancement is predicted to be stronger at the LHC.

PHENIX has extracted the cross-section for open charm in the momentum range  $pt < 2$  GeV/c via inclusive electron spectra<sup>15</sup>. However this result required a large subtraction of background electrons from other sources, and at moderate to high-pt the spectrum receives contributions from both open charm and beauty. The proposed upgrade separates charm and bottom production with high accuracy. Charm may contain a thermal contribution while bottom could serve as a reference since open beauty should be less affected by pre-equilibrium production.

### 2.3.3 $J/\psi$ Suppression

The suppression of  $J/\psi$  has been a long sought after signature of the plasma<sup>16</sup>.  $J/\psi$  that would form from  $c\bar{c}$  pairs are either screened by the plasma or are broken up by interactions with semi-hard gluons. To quantitatively understand suppression requires knowledge of the initial production of  $c\bar{c}$  pairs. The effectiveness of a deconfined medium in preventing the formation of  $J/\psi$  can be quantified using the ratio  $J/\psi / (\text{open charm})$ .

### 2.3.4 Other Physics Topics

The Si vertex upgrade will help other physics programs in PHENIX. Simulations of these topics have not yet been done to quantify the level of improvement. The upgrade will

- narrow the mass-resolution for di-muon and di-electron invariant mass, opening up the possibility of upsilon spectroscopy. The mass resolution for reconstructing the  $\Upsilon$  via the  $\Upsilon \rightarrow e^+e^-$  decay is estimated to improve to  $\sim 60$  MeV/c, which will enable PHENIX to separate the 1S, 2S, and 3S excited states of the  $\Upsilon$ , (provided there is sufficient luminosity).
- The  $J/\psi$  resolution in the muon arms will be improved using a vertex detector, from  $\sim 130$  MeV down to  $\sim 100$  MeV. This is important for separating the  $\psi'$  from the  $J/\psi$ - much of the physics is cleaner to interpret for the  $\psi'$  since it does not have such a large contribution from feeddown like the  $J/\psi$  does.

- provide an estimate of the contribution of charm to the e+e- continuum. This will be necessary in the search for thermal production of e+e- pairs.
- improve high-pt tracking in the central arm by providing confirming hits close to the collision point. This will reduce background contributions to the high-pt track sample.
- increase the signal to background for all muon-pair combinations in the muon arms by removing muons from long-lived pion and kaon decay.
- measure multi-strange baryons.

### 3 Simulations and Required Performance

The performance requirements for the detector are

- ability to match tracks from central arm and muon arm to hits in multiple layers of the Si detector.
- sufficient position accuracy so that the displacement resolution of the track with respect to the collision point is less than the  $c\tau$  of charm and beauty decays, i.e. a resolution less than 100 $\mu$ m, preferably at the level of 30-50  $\mu$ m.
- for tracks at mid-rapidity the resolution needs to be predominantly in the  $r\phi$  direction, for tracks at forward/backward rapidity good resolution in both  $r\phi$  and z are required

A variety of simulations and first principle calculations have shown that the displacement resolution is dominated by the position accuracy of the two inner Si layers and by the amount of multiple-scattering between the collision point and these two position measurements. A first order guide of how well the measurement of two positions can be extrapolated back to the collision point is

$$s^2_{DCA} \approx \frac{(\Delta x_1^2 + \Delta x_2^2)}{separation^2} r^2 + \theta_{ms}^2 r^2 + \Delta x_1^2$$

where  $\Delta x_1$  and  $\Delta x_2$  are the two position measurements from the inner two Si layers, r is the distance from the collision point to the first layer, separation is the separation between the first two layers, and  $\theta_{ms}$  is the multiple-scattering angle due to material in the beam-pipe and first-layer of Si. The first two terms approximate how well the direction of the track can be extrapolated to the collision point while the last term estimates the additional uncertainty in locating the position of the track. This equation is meant as a guide only and is superseded by simulations.

To minimize the DCA resolution, the first layer should be as close to the collision point as is practical (small r), and the first layer plus beam-pipe should be as thin as possible. It should be noted that over a broad range of momentum multiple-scattering dominates (2<sup>nd</sup> term above) and that the accuracy of the hit measurement is not the determining factor (1<sup>st</sup> and third terms).

After exploring different configurations we decided on a semi-realistic layout with reasonable thickness and positions for its Si layers (figures 1 and 2). We plan to iterate on the design, bringing in necessary details of the mechanics, layout, cooling, cabling etc.. The detector has four concentric barrels of silicon which occupy the central 30 cm along the beam axis. The outer three barrel layers are Si strip detectors placed nominally at r=10cm (barrel 4) r=8cm (barrel 3) and r=6 cm (barrel 2). The inner barrel of silicon at r=2.5 cm is composed of pixel detectors (barrel 1). The beam-pipe is at r=2.0cm and is 500 $\mu$ m Be. The endcaps comprise of four lampshade shaped disks of pixel detectors. The inner radius for each disk is at 3.5cm

For the simulations we have used two nominal thickness for each layer: 1 and 2% radiation length. This includes detector, readout and cooling in a simplified one-volume effective layer. From a survey of built detectors a radiation length of 1.5% should be achievable while 1% is very aggressive. We are striving to minimized this thickness, in particular for the critical first layer.

The pixel detectors for the inner barrel layer are planned to have a segmentation of 50 $\mu$ m by 425 $\mu$ m while the endcaps have a larger footprint of 50 $\mu$ m by 2000 $\mu$ m. The strip detectors (outer 3 layers) have a 80 $\mu$ m

pitch and a strip length that is 3cm long. As described more fully in Section 4.2, the sensor has two readout strips (x and u) which provides localization to  $80\mu\text{m}$  by  $800\mu\text{m}$ . This is not much larger than a Si pixel but requires a low occupancy environment to make the projective geometry work.

In order to maintain the occupancy below 10% in central Au-Au collisions, the area of the sensitive elements in barrel layer 2 should be smaller than  $2.9\text{ mm}^2$ . This is met by the candidate strip detectors that have a  $80\mu\text{m}$  pitch, 3cm length for a surface area of  $2.4\text{mm}^2$ . The occupancy is lower in the outer two barrel layers.

In the following sections, we describe the simulated performance of the proposed silicon vertex detector consisting of a central barrel region matched to the PHENIX central arms and two endcaps matched to the PHENIX muon arms. The simulations have been run within PHENIX's implementation of GEANT, PISA. For convenience, we have separated each of the next sections into measurements possible with the central PHENIX arms plus the silicon barrel and those possible with the silicon endcaps and PHENIX muon arms. However, there are some measurements listed below that require all of PHENIX's capabilities used in unison.

### 3.1 Open Charm Measurement

#### Barrel: $D \Rightarrow e+X$ , $D \Rightarrow K+\pi$

Open charm spectra and yields are key for the physics goals of spin gluon structure physics, structure function work in pA reactions, and as probes of the early stages of heavy-ion collisions. For the latter the goal is to confirm that the excess of electrons observed<sup>15</sup> does indeed come from charm decay, and to then extend the reach in pt to measure the energy-loss of open charm at high pt.

The four layers of the central silicon barrel provide an accurate measurement of the trajectory and impact parameter of tracks near mid-rapidity. Single electrons at different momenta were simulated through the strawman vertex detector. This simulation was run at zero-field and the hits from the electrons tracked back to calculate the transverse distance-of-closest approach (DCA) to the known point-of-origin.

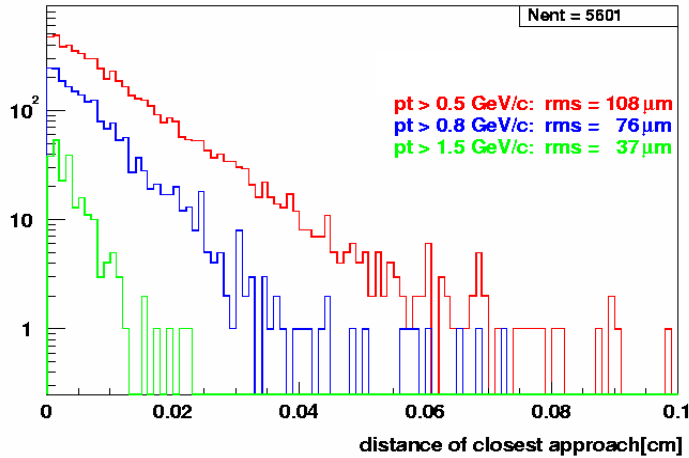


Figure 4, the distribution of distance of closest approach to the collision point for electrons passing through the central barrel.

For all cases the DCA resolution is better than or comparable to the  $c\tau$  of charm and beauty decays. The power of this resolution is seen by comparing the distribution of DCA from charm, beauty and Dalitz decays of  $\pi^0$  in figure 5. The spectra were generated from p+p events (PYTHIA) passed through PISA.

In the bottom panels of figure 5 are the DCA distributions for electrons above 1 GeV/c. A DCA cut of 200  $\mu\text{m}$  removes the majority of Dalitz contribution from the electron yield. Note this is the momentum of the electron and given the large Q-value of the D-decay, these electrons predominantly come from low-momentum D's. Since beauty decays have longer lifetimes, the electrons from B decays dominate at large DCA values. By fitting the full DCA distribution with the expected shapes from the different ct we should be able to simultaneously extract charm and beauty yields.

This process is more difficult at electron momenta closer to 500 MeV/c but even at this momenta charm dominates the DCA distribution above 200  $\mu\text{m}$  for Si thicknesses between 1 and 1.5% radiation length.

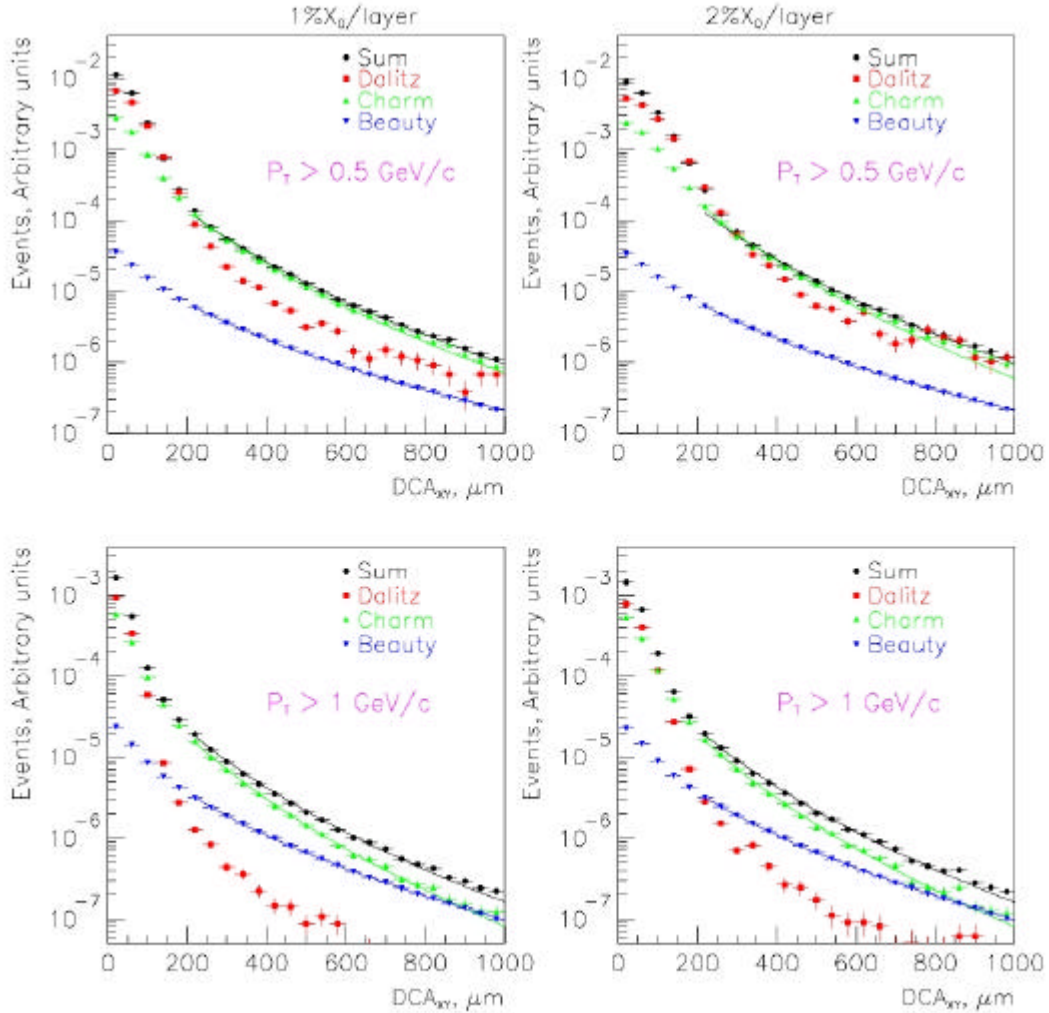


Figure 5, DCA distribution for electrons from Dalitz, charm and beauty decays simulated through four 1% Si layers on the left and four 2% layers on the right.

At higher pt we will measure charm spectra via hadronic decay channels. For these momenta electrons from B-decay dominate the charm yield (see section 3.3). As an illustration of hadronic decay we plot the three body invariant mass distribution for  $D \rightarrow K\pi\pi$  in Figure 6. This simulation is for p+p from Pythia events embedded in a HIJING Au+Au background event. Simultaneous cuts (find values) are placed on three displaced tracks and in addition the parent D must point close to the collision vertex. These cuts produce a reasonable signal/background. The challenge will be the low rates at high-pt. As an estimate if

we assume Au+Au 4\*blue-book luminosity, 50 full days/year, yield Au+Au= AA\*(yield p+p) then the  $D \rightarrow K\pi$  above  $pt > 4$  GeV/c will produce into the PHENIX acceptance 30kevents/year in p+p running and 10k events/year in Au+Au. This estimate is very preliminary and requires more study regards TOF and aerogel acceptance. Triggering on these events is discussed in section 3.x.

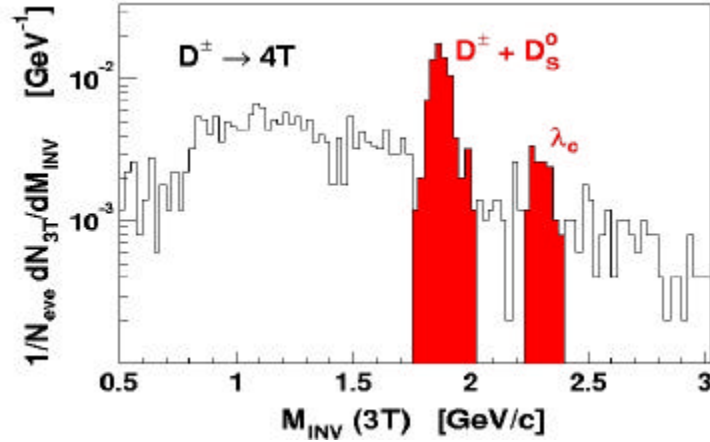


Figure 6. The three body invariant mass distribution is shown for  $D \rightarrow K\pi\pi$ . This simulation is for p+p from Pythia events embedded in a HIJING Au+Au background event.

**Endcaps:  $D \rightarrow \mu + X$ ,  $D \bar{D} \rightarrow \mu + e + X$ ,  $D \bar{D} \rightarrow \mu^+ + \mu^- + X$**

Each silicon endcap detector has four layers of pixel detectors which measure the trajectory of particles within the nominal rapidity acceptance of the muon arms. The impact parameter of each track is determined accurately along the Z (beam) direction. For each detected muon, the impact parameter is used to eliminate muons that come from pion and kaon decays. These long-lived decays are the primary source of background muons.

Contrasted with these background muons are "prompt" single muons, which come from more short-lived decays, e.g. open charm and beauty. For transverse momenta below  $\sim 5$  GeV/c the prompt muons are primarily from semi-leptonic charm decay. Other processes which produce prompt muons, such as  $J/\psi$  or Drell-Yan decays to muon pairs, have much smaller cross-sections times branching ratios. Muons from B decays become important only at larger transverse momenta.

The PYTHIA event generator was used to simulate semi-leptonic charm decays to muons. The total charm pair cross-section was set at 350 microbarns, which is consistent with recent NLO theoretical calculations and with the published PHENIX measurement at a somewhat lower energy. The decay muons were tracked through the proposed silicon vertex detector and then through the muon spectrometer using PISA.

The mean decay vertex of the detected muons is 785  $\mu\text{m}$  from the interaction vertex. This is  $\sim 2.5$  times larger than the proper decay length of semi-leptonic charm decays (318  $\mu\text{m}$ ), due to the lorentz boost. The impact parameter resolution for these muons ranges from 92 to 115  $\mu\text{m}$  (check), depending on how many total layers of silicon are transversed. By requiring that the muon vertex is within 1cm of the collision point we remove many of the muons from pion and kaon decay while retaining prompt muons from charm and beauty.

The  $pt$  distribution of muons that decay within 1cm of the collision vertex shown in Figure 7. This cut reduces the muon background from light mesons to one order of magnitude smaller than muons from charm. Note that the removal of the muon background from pion and kaon decays could be achieved with a

detector with less spatial resolution. The resolution requirement is driven by the physics program of measuring open beauty (see next section).

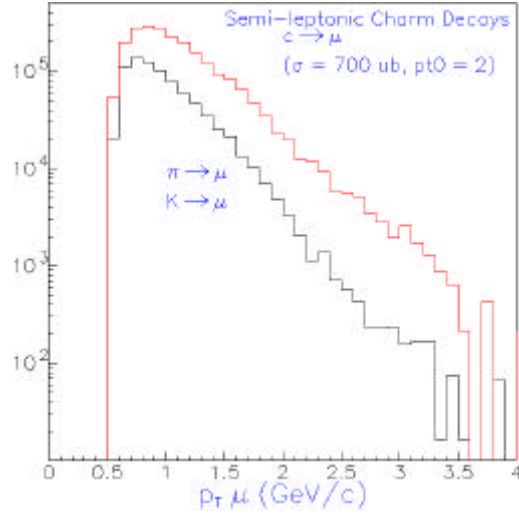


Figure 7. The  $p_t$  distribution of muons that decay within 1cm of the collision vertex.

To calculate the rate of collecting charm data we assume a 350 microbarn cross-section, average p-p luminosity of  $8 \times 10^{31}$ , 48 days of beam, acceptance time branching ratio of  $5.6 \times 10^{-5}$  and two muon arms, about  $1.4 \times 10^7$  semileptonic charm decays would be recorded. This rate of  $\sim 300,000$  per day is before application of a vertex or impact parameter cut.

Since charm is produced in pairs, coincidence measurements of opposite-sign lepton pairs may serve to further enhance the signal to noise in pp and pA reactions. One could use vertex identified muon-electron coincidences to obtain a clean charm pair signal in the rapidity interval midway between the PHENIX central and muon arms.

### 3.2 Open Beauty Measurements

B meson production, while much rarer than D production, is somewhat simpler to measure. The challenge is the relatively low rate. There seem to be at least two possibilities;

- Since beauty mesons have a larger lifetime than charm mesons, it is possible to extract the beauty yield from the distribution of decay distances. At large transverse momentum beauty decays dominate the DCA distribution.
- The decay channel  $B \Rightarrow J/\psi$  produces  $J/\psi$  that are displaced from the collision that can be used to extract the B-yield

#### **Barrel: $B \Rightarrow e + X$**

For momenta greater than 3 to 4 GeV/c electrons with displaced vertexes are dominated by beauty decays. This is clearly seen in figure 8. By placing a DCA cut on the order of  $150\mu\text{m}$  we should be able to cleanly separate electrons from beauty from all other sources. Note that at these momenta it will not be possible to extract a charm source using electron decay. As discussed in the previous section this will be done via the hadronic decays of charm.

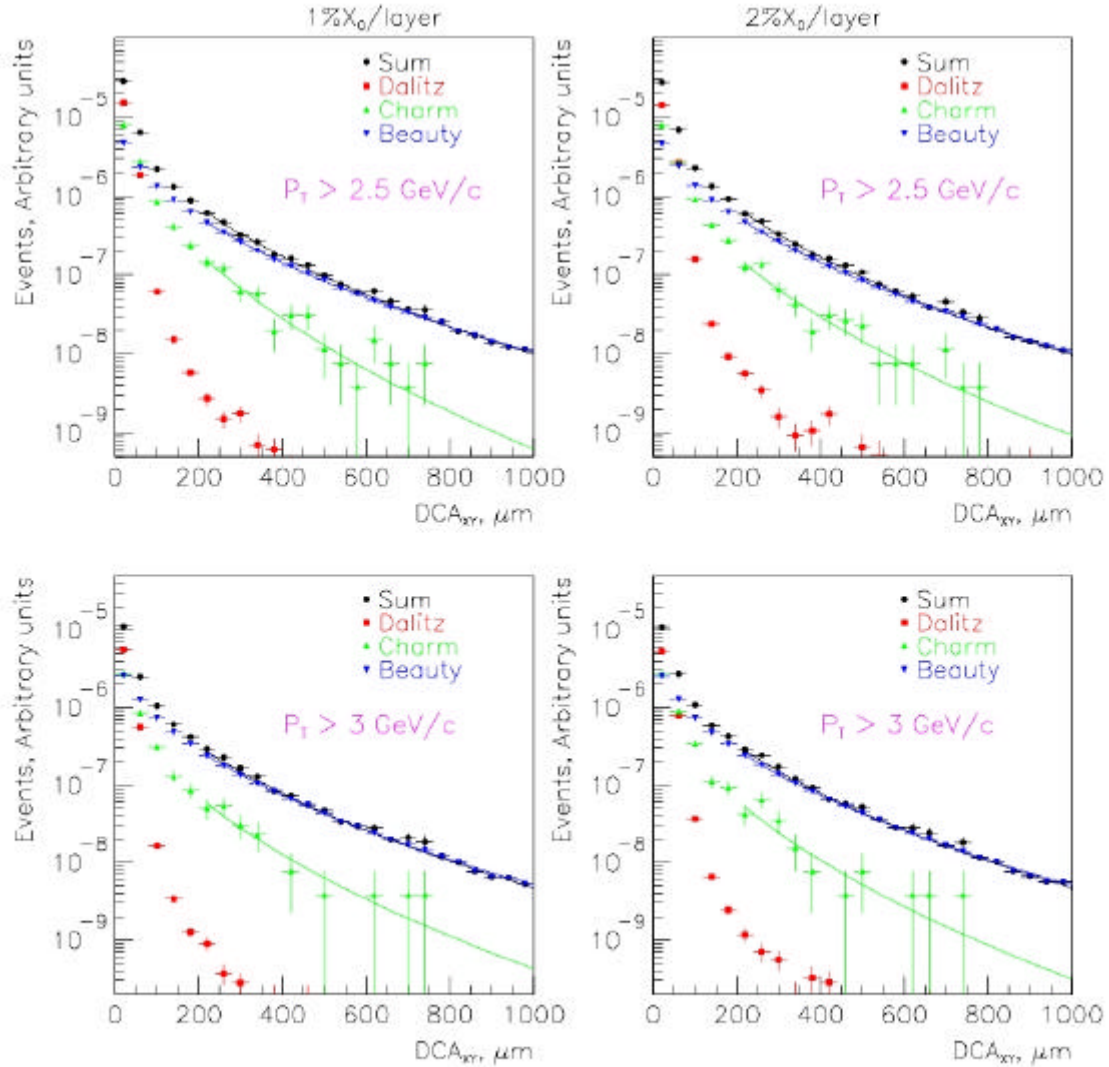


Figure 8, DCA distribution for electrons from Dalitz, charm and beauty decays simulated through four 1% Si layers

For the rate calculation we assume Au+Au 4 blue-book luminosity, 50 full days/year, yield  $Au+Au = AA \cdot (\text{yield } p+p)$ . With these assumptions the decays  $B \Rightarrow e+x$  with electron  $p_T > 4 \text{ GeV}/c$  will produce 320k events/year in p+p running and 125k events/year in Au+Au.

Beauty decays are also accessible through the semi-leptonic decay channel to muons. Since the muon arms have a relatively large acceptance compared with the central arms, sufficient statistics can be achieved with blue book luminosity.

**Endcaps:  $B \Rightarrow J/\psi \Rightarrow \mu^+ + \mu^-$**

Applying a vertex cut on each reconstructed  $J/\psi$  has been used successfully to identify B-production in experiments at lower energies<sup>17</sup>. Since the B cross-section is larger at RHIC energies, the measurement should be easier. As the average  $p_T$  of  $J/\psi$  from beauty decays is much larger than for prompt  $J/\psi$ , a  $p_T$  cut could also be used to enrich the beauty sample.

Pythia was used to simulate  $B \Rightarrow J/\psi \Rightarrow \mu^+ \mu^-$  decays. The resulting muons are tracked through the silicon and muon spectrometers using PISA. The muons have an impact resolution of  $\sim 55\mu\text{m}$ , significantly better than muons from D decays, due to their larger average momentum. The pair vertex resolution is  $\sim 133\mu\text{m}$ , while the mean decay length is  $\sim 1.1\text{mm}$ . With a downstream pair vertex cut of 1mm, 39% of the B decays are retained, while the prompt  $J/\psi$  are attenuated by a factor of  $2 \times 10^{-4}$ . Figure 9 shows the reconstructed Z-vertex distribution for the  $J/\psi$  from B decays as well as prompt  $J/\psi$ .

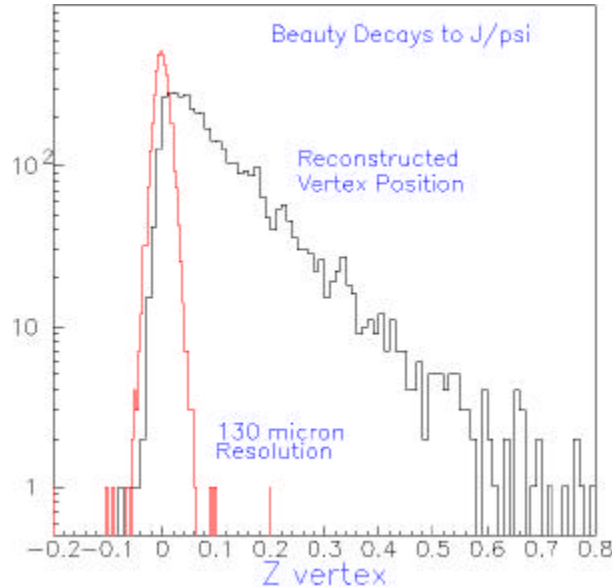


Figure 9 The reconstructed Z-vertex distribution for the  $J/\psi$  from B decays (solid line) and the prompt  $J/\psi$  (dashed line).

We have assumed a B cross-section of 2 microbarns and 3 microbarns for  $J/\psi$  production. The branching ratio of 1.2% for  $B \Rightarrow J/\psi$  has been previously measured. The total acceptance for these events using both muon arms is  $\sim 11\%$ . The rate is calculated by assuming a 2 microbarn cross-section, average p-p luminosity of  $8 \times 10^{31}$ , 48 days of beam, acceptance time branching ratio of  $7.8 \times 10^{-5}$  and two muon arms. With these assumptions, about 50,000 beauty decays would be recorded. This rate of  $\sim 1,000$  per day is before application of a vertex cut. With a realistic vertex cut of 1mm, 400 events per day could be reconstructed. Even with a factor of 10 lower average luminosity, an excellent beauty measurement is possible.

### 3.3 Trigger Plans

We plan to use the lv11 single electron, single and di-muon triggers as the main physics trigger for the vtx. Higher level triggers could be a lv12 displaced track trigger, possibly similar to the trigger used by CDF. CDF has implemented the trigger in hardware so is optimized for speed. For PHENIX this could be ported to lv12.

The CDF algorithm functions in three steps (translated into PHENIX language); 1) outer tracks are found from either drift chambers and/or PCs. This provides a beginning  $pt$ 's and  $\phi$  for each track. These tracks are then propagated to the vtx detector. A template matching algorithm is used to associate hits with the seed tracks. Valid patterns of super-hits are pre-stored in a lookup table and these patterns are compared with all the hits from the vtx. A super hit is a collection of hits the size of which is a compromise between speed and accuracy. Patterns that match with super-hits are also checked to see if there is a seed track that matches to the pattern.

The original hits that contribute to the matched pattern are then passed to a fast, linear fitting algorithm that provides the dca, pt, and phi of the track. In CDF this algorithm is implemented in hardware and works within 20 microseconds. The rejection factor reported by CDF for displaced tracks is over 200. An ongoing R&D program is to explore the feasibility of such an algorithm for PHENIX in full Au+Au collisions and to establish an estimate of the rejection factors.

The aerogel lvl1 trigger is a candidate trigger for the channel  $D \Rightarrow K + \pi$ ,  $pt > 4 \text{ GeV}/c$ . This trigger is part of the proposed aerogel upgrade and would fire on pions  $> 2 \text{ GeV}/c$ . These events would then be passed to the lvl2 triggers of displaced vertexes and/or high-momentum tracks.

### 3.4 Event Rates

The event rates in the previous sections are summarized below. They assume average p-p luminosity of  $8 \times 10^{31}$ , Au+Au 4 blue-book luminosity, 50 full days/year, yield  $\text{Au+Au} = AA * (\text{yield p+p})$ . All observables would benefit from the increased luminosity in the RHICII proposal. Difficulties in triggering the  $D \Rightarrow K + \pi$ ,  $pt > 4 \text{ GeV}/c$  channel may reduce the collected counts by up to a factor of ten.

Observable	Counts per RHIC pp Run	Counts per RHIC Au+Au Run
$D \Rightarrow K + \pi$ , $pt > 4 \text{ GeV}/c$	30k	10k
$D \Rightarrow \mu + X$	$1.4 \times 10^7$	$0.4 \times 10^7$
$B \Rightarrow e + x$	320k	125k
$B \Rightarrow J/\psi + \mu^\pm$	20k	6K

### 3.5 Matching to Spectrometers

Track matching between the endcaps and the muon system spectrometers was studied by using hijing Au-Au central collisions in a PISA simulation. A muon track was embedded in a hijing event. The muon track was found in station 1 from the muon tracker by demanding that the muon reached the middle of the MUID, i.e. muon energy was  $> 2.5 \text{ GeV}$ . The distribution of the muon hits in station 1 was found to be  $\pm 2 \text{ cm}$  due to multiple scattering in the central magnet steel. We then projected all tracks in the central region to station 1 and found that on average 3 tracks projected into the vicinity of the muon track. Each of these three tracks came from the primary vertex and the displaced muon track was easily identified with a vertex cut of 1mm.

### 3.6 Integration with Phenix

The proposed vertex detector matches and extends the capability of the existing spectrometer arms. In addition a joint HBD/TPC is being proposed to sit outside the vtx. The Detector Advisory Committee recommended studies exploring the impact of the VTX on the HBD/TPC with the possibility of standalone running for either detector. These studies are in progress and our workplan is outlined here.

Tracking from the VTX should help the TPC and hence may Dalitz rejection. However the VTX is a background source of electrons to the proposed HBD detector. We are investigating how to remove many of these electrons via analysis cuts

- veto conversions should be removable from the outer three layers of the vertex detector since tracks from conversions will not have hits in the inner layers.
- the remaining conversion pairs from the first layer might be removed if the tracks intersect at the first layer. Since the occupancy of the first layer is  $< 1\%$  this should effectively remove conversions from the inner layer as well.
- we may be able to reject conversions in the beam-pipe by removing electron pairs if the tracks intersect at the beam-pipe.

## 4 Technical aspects of the Proposed Vertex Detector

### 4.1 Hybrid Pixels, First Barrel Layer

Hybrid active pixel detectors have been developed at CERN and FERMILAB since the late 1980s, for their application in experiments at the Large Hadron Collider (LHC)<sup>18</sup>. Along this path, a series of pixel readout chips of increasing complexity and performance was designed. Several intermediate applications in heavy ion and high energy physics experiments were realized. Experience with pixel detector systems was gained in tracking stations in the fixed target experiments WA97 and NA57. The first application of hybrid pixel detectors in a collider experiment, pioneered by the DELPHI collaboration at LEP for its Very Forward Tracker, operated from 1995 until the end of LEP in 2000.

#### 4.1.1 Readout Chip

PHENIX will use the ALICE1 readout chip<sup>19</sup> developed by the CERN EP microelectronics Group. This chip will be used in the Inner Tracking System of the ALICE experiment<sup>20</sup> and PHENIX has the opportunity to participate in one of the production runs. It is also the building block of the silicon pixel telescope of the NA60 experiment at the SPS. With an agreement between the ALICE and RIKEN readout chips and sensors are provided to RIKEN in a common production effort.

The ALICE1LHCb pixel readout chip is currently being fabricated in a commercial 0.25 $\mu\text{m}$  CMOS process. Its analog and digital circuitry operates with a 1.6V power supply. The total static power consumption per chip is about 500mW. This active area of the chip of 13.60mmx12.80mm is divided into 8192 pixel cells of 50 $\mu\text{m}$ x425 $\mu\text{m}$  area that are arranged in 32 columns by 256 rows. Every pixel cell itself is divided into an analog and a digital part. The schematics of the components are shown in Fig.x.

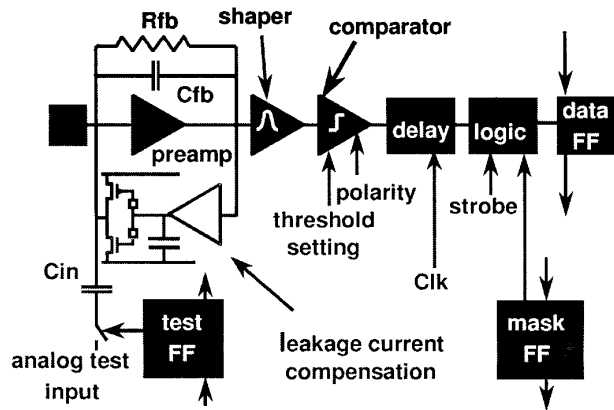


Figure 10 ALICE1 schematic pixel electronics (check this is most up to date)

The analog front-end consists of a pre-amplifier followed by a shaper stage with a peaking time of 25ns. A mask flip-flop allows the pixel to be disabled. A discriminator compares the output of the shaper with a threshold provided globally across the chip. Each pixel contains three logic bits that can be used to finely adjust the thresholds individually for every pixel to provide pixel-to-pixel threshold uniformity over a full detector system. The outputs of the discriminators in the pixel matrix provide a fast-OR and a fast-multiplicity signal which is output off-chip. In every pixel, the discriminator output is fed into the digital part of the cell. The first stage consists of two digital delay units that store a hit for the duration of the trigger latency. Each delay unit consists of an 8-bit latch which, on receipt of a hit from the discriminator, latches the bit-pattern present onto an 8-bit bus. This pattern is the Gray-encoded contents of an up-down counter whose state changes synchronously with the clock and has an adjustable modulo n. The result of the trigger coincidence is loaded into the next-available cell of a 4-event FIFO, which acts as the multi-

event buffer and de-randomizer. This FIFO is read/write addressable by means of two 4-bit busses which carry Gray-encoded patterns. The contents of the FIFO cells waiting to be read out are loaded into a flip-flop by the Level-2 trigger in ALICE. The flip-flops of each column form a shift register, and the data is shifted out using the system clock. Five latches inside each cell switch on or off the test input to the front-end, mask or activate a pixel and provide three bits of threshold adjustment. The latches have been designed to be resistant to single-event upset.

Using the two delay units, each cell has the capability of simultaneously storing two hits for the trigger latency. The 32 columns are read out in parallel. Using a 10~MHz clock, a complete event is read out from the chip in 25.6  $\mu$ s. The peripheral logic of the chip contains the counters to address the delay units and the FIFOs. The configuration of the logic and the matrix of pixel cells is performed by means of a serial interface following the IEEE JTAG standard.

#### **4.1.2 Sensor/Readout Hybrid**

A pixel chip assembly is an ALICE1 pixel readout chip bump-bonded to a pixel sensor chip. Their relative alignment is assured by the requirement that the 20 $\mu$ m bonding pad of each readout pixel matches that of the corresponding sensor pixel, for a solder bump to form between them. The sensitive area is a 32 x 256 matrix of 50 $\mu$ m x 425  $\mu$ m pixels in the sensor chip, matching the dimensions of the pixel readout chip. This active matrix of 13.60mm x 12.80mm is surrounded by a guard ring and a scribe line, adding 560 $\mu$ m on all four sides. In practice, this may slightly vary, depending on the precision of the dicing and the width of the cut. The sensor chip's thickness is 300 $\mu$ m.

After bumping the readout to the sensor, both Si components are thinned to a target thickness of 150  $\mu$ m each. The contract with ALICE is to provide RIKEN with enough thinned to populate the first layer of the barrel.

#### **4.1.3. Control Card**

Geometrically eight readout chips might comprise a phenix ladder. Two ladders would then be placed to end-to-end to make one azimuthal slice of the inner layer. Since the readout chips operate at 10 MHz, a controller chip on the end of the ladder could address each chip in turn, i.e. read the first 32-bit word from chip one, the first word from chip 2 etc.. If the controller chip functions at 40 MHz then the event is readout in 52  $\mu$ s which is too long for PHENIX needs. If the controller exceeds 80 Mhz then the readout time can be reduced to 25.6  $\mu$ s.

ALICE has designed a readout card that comprises of three chips, an analogue power supply chip, a controller chip (PILOT) and an optical driver for the output. These chips are mounted on a thin circuit board. To decrease the time to read an event PHENIX has two options, either a redesign of the existing PILOT chip to move from 40 to 80 MHz or to replace the ALICE pilot chip with a commercial, fast, radiation-hard FPGA. The primary advantage of the FPGA would be on-ladder zero suppression of the pixel chip readout. This would reduce the data volume the receivers would be required to deal with. Further study will be needed to determine which FPGA technology is most applicable to the problem and which manufacturer provides workable solutions, as well to address issues of power consumption, heat load, radiation hardness, etc..

#### **4.1.3. Electrical Ladder**

The technology of making connections between chips has undergone an explosive growth in industry over the past 5 years. Our requirements of small pitch traces, lightweight signal bus, good thermal conductivity and low-cost for assembly are the same factors that commercial electronics have used to drive industrial connect technology. This is fortunate because we can ride the coat-tails of industry.

ALICE will use a multi-layered kapton cable with Al traces and kapton cable is being used by ALICE. Each chip requires 32 signal traces, so for eight chips per ladder, the trace density is high necessitating

trace widths on the order of 100 microns. The wire bonds go from the readout chip, up over the sensor to be connected to the bus. This is shown in figure 11.

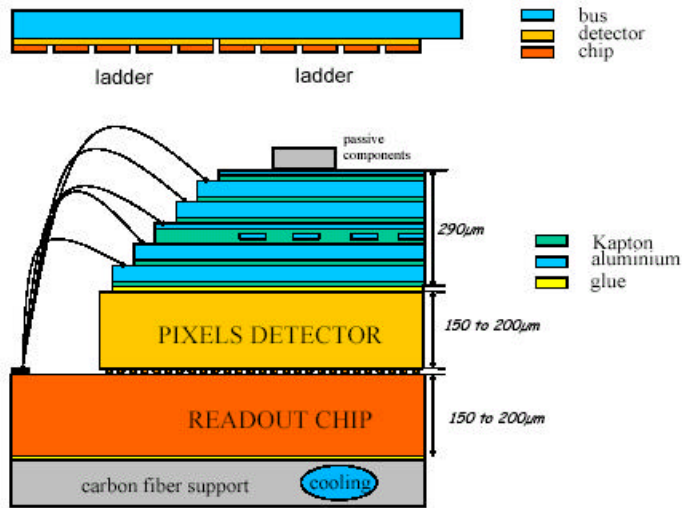


Figure 11, the assembly of the sensor, readout and signal bus used by ALICE

An alternative option for the bus is a thin ceramic (BeO) with multi-layered signal and analogue ground and power traces. The ceramic technology was chosen in 2002 by CDF and D0. The BeO ceramic has better heat conductivity, smaller thermal expansion. This may make it possible to place the bus between the readout chip and the carbon fiber support. Such a configuration may lead to lower assembly costs.

## 4.2 Silicon strips

### 4.2.1 Sensors

The outer three barrel layers of the silicon detector will be instrumented by silicon strips, most likely a new form of the detectors developed and fabricated by BNL instrumentation<sup>21</sup>. Tests of these devices have started and will continue through 2003. The BNL detectors are 3x6cm in size that are segmented as pixel detectors. The pixels are connected by readout strips currently configured as two sets of read-out strips placed longitudinally and diagonally. This provides simultaneous x-u readout from a single surface. At low-occupancies this projective geometry localizes a hit to within a pad of 80x800µm. Each strip detector has ~1500 channels (375 channels per end, 2-readouts per end and two ends per detector). Depending on final layout plan, the total number of channels is 200 to 300K.

Beam tests have been carried out at KEK. An example set of position information is shown in figure 12. The particles cross the sensors at different channels and a clear signal is discernible above the background.

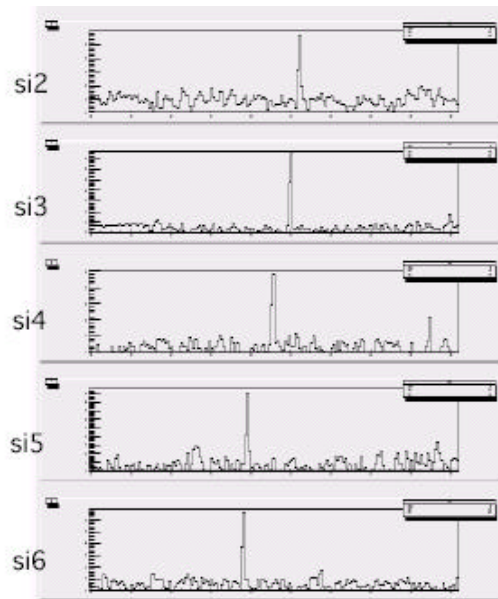


Figure 12, channel position histograms for five silicon strip detectors in a test beam

The residual of hit position from the found track provides information on the position resolution. This is shown in Figure 13 for one sensor. The sigma of the residual distribution is  $\sim 40$  micron for those sensors that are 400 micron thick while the resolution is larger,  $\sim 50$  micron for thinner sensors (250 micron thick). Currently the resolution is larger than expected and the continued improvement of the sensors is the topic of ongoing R&D.

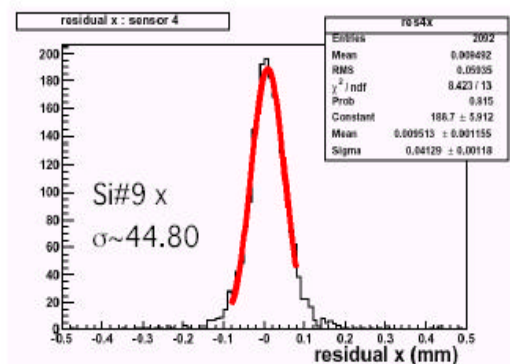


Figure 13 hit residual from tracks found using the silicon strip detectors in a test beam

#### 4.2.2 Strip readout

The leading candidate for the strip readout is the SVX4 chip developed at Fermilab<sup>22</sup>. The SVX4 uses 0.25 $\mu$ m CMOS technology which is broadly available. It is a 128 channel chip with a 46 deep pipeline cycled by the beam-crossing clock. The rise time is on the order of 60 ns. A collaboration has been established between ORNL/RIKEN and FNAL and it may be possible to participate in a production run of these chips in the summer of 2003

Considerable R&D is still required to integrate the svx4 into PHENIX DAQ and to design the ladder for the strip layers. Other concerns include the high heat load of the chip and coupling issues with the sensor. One option is to frequently reset the svx4 since the sensor requires DC coupling. The effects of leakage current may also be reduced if the sensors are cooled to below room temperature.

The SVX4 chips may be loaded onto a ceramic (BeO) multi-layered board which has good heat conductivity and low thermal expansion. Five 6cm sensors nicely fill up 30 cm in z – therefore natural to think of a FEM/DCM as reading out a  $\phi$ -ladder and controlling 60 readout chips per ladder.

#### 4.3 Endcap Hybrid Pixels

The endcaps are planned to be instrumented by Si pixels. It is strongly advantageous to use the same detector technology as for the barrel layer. Because of the greater surface area of the endcaps, we are currently investigating whether the footprint of each pixel can be increased to have fewer pixels per sensor and readout chip. The current planned pixel size ( $> 2\text{mm} \times 50\text{ microns}$ ) is a compromise between channel count (heat and cost) and occupancy. A key issue will be how much the noise increases as the capacitance of the pixel increases.

For the readout chip one option is to use the LHCPIX1 chip as the baseline rather than the ALICE1 chip since the LHCPIX1 chip runs at 40 MHz compared to 10 MHz for ALICE1. These two chips were developed by the same team, have the same functionality, and the same control interface. A similar controller card would be used for the endcaps as will be used for the barrel pixels. Again the possibility of zero-suppression is a strong motivation to use a FPGA in this controller card.

In addition if the chip is designed with widely spaced bumps then the bump bonding will be easier. An attractive possibility currently under investigation is to bump-bond both the sensors to the read-out chips and the read-out chips to the electric bus in one assembly step. This could dramatically reduce assembly costs but placed an increased premium on quality control to ensure high-yield.

#### 4.4 Channel Count

	Channels	Occupancy
barrel 1 <sup>st</sup> :	1.3 M	<1%
barrel 2 <sup>nd</sup> :	92 K	12%
barrel 3 <sup>rd</sup> :	123 K	7%
barrel 4 <sup>th</sup> :	154 K	5%
endcaps;	2.8 M	<3%

#### 4.5 Mechanical structure and Cooling

The LANL group has initiated contact with the firm HYTEC to discuss the conceptual design. HYTEC are the mechanical design team for the ATLAS silicon vertex detector. For PHENIX they have designed the station 1 muon detectors and the station 2 spider and also did the finite element analysis of the station 3 octants. Hytec was commissioned to do a preliminary design study, from which we quote the following from their report<sup>23</sup>.

“The basic requirements for the PHENIX tracker are given in the outline below.

1. Clamshell Design:
  - i. Separates into two halves along the vertical axis
2. Detector Coverage:
  - i. Hermeticity: single overlap circumferentially

- ii. 160° coverage in each half of barrel section
- iii. 4 layers of pixels and/or strip detectors in barrel section
- iv. 180° coverage in each half of the end cap sections
- v. 4 layers of pixel detectors in end cap sections
- 3. +/- 40° Envelop for HBD/TPC maintained around barrel section
  - i. End cap pixel disks, utilities, and barrel detector end support are outside of envelope
  - ii. Main clamshell support structure is inside of envelop, but less than 0.5% RL
- 4. Radiation length (RL) of 1% or less for each detector layer (includes: detectors, structure, and utilities)
- 5. Dimensional and structural stability of less than 25 μm for detectors and 100 μm gravitational structural stability of entire tracker
- 6. Utility Routing:
  - i. Along barrel end support for barrel region
  - ii. Radial at pole tips for the end caps
- 7. Mounting of Tracker:
  - i. Off of magnet pole tips
  - ii. Tracker to behave as a rigid body structure
  - iii. Operating Temperature: Room temperature (or possibly 0°C option?)

#### 4.5.1 Material Selection

“The use of Graphite Fiber Reinforced Plastic (GFRP) sandwich composites for the base structure is suggested because of the substantial gain in the stiffness to weight ratio. Fiber selection for the GFRP was deferred to the candidate that is most readily available and at a reasonable cost. M55J is the most widely used standard in the composites industry, and so it was used throughout the remainder of the structural study.”

#### 4.5.2 Structural Analysis Summary

“The structural analysis of several concepts revealed the following observations. Use sandwich composites for the frame structure instead of solid laminates or some combination of both. Radiation length requirements can be met with GFRP sandwich composites, and sandwich composites have been show to have better stiffness to weight ratios. Outer frame structure should be a single diameter size across all three detector regions and as large a diameter as possible for the given envelope for the PHENIX Pixel Detector upgrade.

- Stability and alignment requirements can be attained with a clamshell design, if sufficient R&D is done on connection issues regarding the two clamshell halves.
- Suggest using an eight-sided shape for the outer structure. The eight-sided shape lends itself to simpler fabrication and allows for better routing of utilities out of the barrel region and end cap regions.
- Structural end disks to close out the tracker support structure are recommended for preventing deformation of the structure under dynamic load inputs at the tracker support points.”

#### 4.5.3 Cooling Analysis Summary

“First order calculations were made for both regions. The results of these preliminary analyses are:

##### *Coolant*

- Use single phase coolant, as opposed to using phase change coolants; this is suggested as a means to significantly simplify the attendant coolant system
- Use perfluorocarbon fluid, C5F12 or C6F14, with the final decision reserved for the final system study
- Flow coolant under turbulent flow conditions to enhance convective heat transfer coefficients, thereby substantially reducing the temperature drop in the coolant film and the gradient in the detector support structures
- Supply the coolant at 20°C inlet, unless sub-cooling of the overall detector is required.

### *End Cap Region*

- Use a flat conical panel sandwich structure for supporting the modules, with module mounting alternating front to back on adjacent panels. Panels are termed sectors, with cooling provided to two adjacent sectors in series. Series connection of adjacent sectors provides modularity of two. Higher modularity may weaken the detector reliability in the event of an isolated failure of a cooling component.
- Construct the structure as a half conical structure, mounted to an outer clamshell sandwich structure.
- Cooling of the End Cap sectors requires removal of nominally 15W per sector, at a comparatively low heat flux. A 2mm inner tube diameter is suggested with a mass flow rate of 9.8g/s for a pressure drop of 6psi per sector. Resulting peak temperature in the surface of the sector should be on the order of 4.5°C or less. Bulk fluid temperature rise for two sectors would on the order of 3°C. Pressure drop can be reduced to under 1psi by using a 3mm diameter cooling tube.
- The preliminary sandwich spacing used in the thermostructural solution was 2mm, with the void between cooling channels filled with carbon foam. The cooling channel is sandwiched between two thermally conductive facings. The facings were assumed carbon-carbon material for reasons of high thermal conductivity and structural stiffness. Further studies of the end cap clamshell panels are suggested for refining the composite sandwich design and to assess thermal strains. However, the thermal strains can be minimized by using a stiff composite sandwich structure.

### *Barrel Region*

In the Barrel Region, we chose to analyze the ladder concept for the silicon strip layer since the total heat load per ladder is greater, 27W versus ~8W per ladder for the pixel layer. The next step in the study will include the pixel ladder design. Continuing the listing of findings and suggestions:

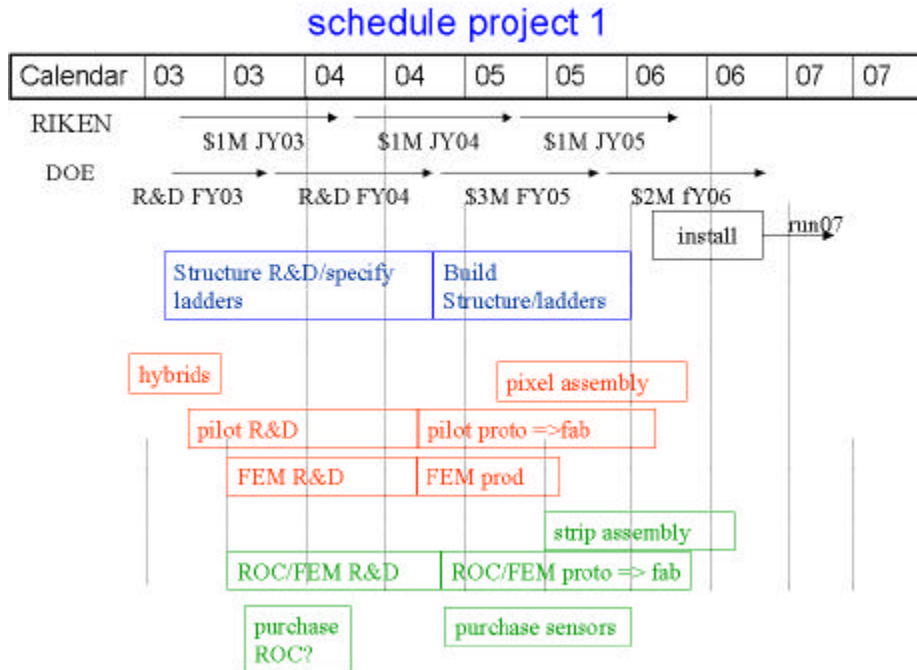
- Use a ladder, or stave, concept supported at its ends by composite rings.
  - One end of the ladder would emulate a simple support and the other a fixed end support. These boundary conditions were chosen to minimize thermal strains.
  - Suggested stave structure comprises a C-C thermal plane for mounting pixel modules, or silicon strip detectors. To add stiffness to the long flat surface, a thin, 0.4mm OMEGA shaped composite is bonded to the back of the thermal plane.
  - Cooling tube is bonded to the back of the C-C thermal plane with a C-C tube support, using a rigid room temperature adhesive
  - Use an Aluminum cooling tube 3mm in diameter supplied with a 23g/s single-phase perfluorocarbon fluid, e.g., C5F12, layer 3 or 4. Estimated bulk fluid temperature rise is 1.1°C for 27W per stave heat pick up. Corresponding pressure drop is approximately 1psi per stave. Estimated peak temperature for a silicon layer (3 or 4) is 8.6°C. Analysis is required for the pixel layer; temperatures may be somewhat higher due to the higher localized heat flux, 0.7W/cm<sup>2</sup> versus 0.35W/cm<sup>2</sup> for the silicon strip layer.
  - Preliminary estimate of bowing for the silicon strip layer, along its 30cm longitudinal axis, due to thermally induced strains is modest. This assumes the coolant is supplied at 20°C. If detector sub-cooling to 0° C is required, the thermally induced strain would increase to 80µm. This thermal component strain for a pixel layer stave, with its higher localized heat flux, may be greater.

“Overall, we feel the system parameters and design approach selected for consideration by the PHENIX collaboration reflects a conservative design with a focus on simplicity to hold R&D and acquisition costs down. The basic structural concepts chosen for supporting the pixel modules are expected to stay within or close to the specified radiation length budget.”

## **5 Schedule and Responsibilities**

For planning purposes the proposed vertex detector is split into two projects: project 1 includes the four layers of the barrel and project two includes the two endcaps. They share common mechanical support and infrastructure.

The draft schedule for project 1. It is planned to install the full barrel in the summer of 2006 ready for run07. A prototype ladder may be ready for installation in summer 2005. The funding for project 1 is proposed to come from RIKEN and DOE.

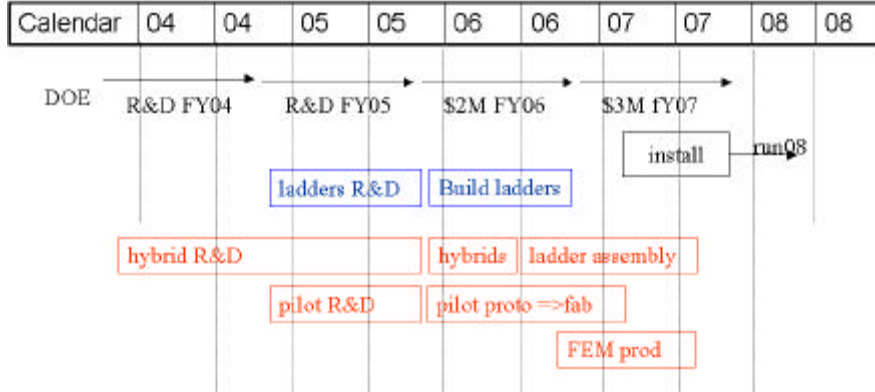


The responsibilities for different parts of project 1 are listed in the following table.

task	institution
mechanical support, cooling	HYTEC/LANL
intearcton. infrastructure	BNL
pixel hybrids,	RIKEN
pixel pilot	ISU
pixel assembly, ladder bus	RIKEN
pixel fem	SUNY-S/B
strip sensors	RIKEN
strip ROC	RIKEN/ORNL
strip FEM	ORNL
strip assembly	RIKEN
DCM II	Columbia

The schedule for project 2 is shown below. It is planned to install the endcaps in the summer of 2007 ready for run08. A prototype ladder may be ready for installation in summer 2006. The funding for project 1 is proposed to come from DOE.

## schedule project 2



The responsibilities for different parts of project 2 are listed in the following table.

task	institution
mechanical support, cooling	HYTEC/LANL
integration, infrastructure	BNL
pixel hybrids, sensor/readout	LANL
pixel pilot	ISU
pixel assembly, ladder bus	LANL
pixel fem	SUNY-S/B
DCM's	Columbia

## 6 Budget

Below is a summary of the construction budget for project 1 and project 2

Construction project 1	Total (k\$)	RIKEN (k\$)	DOE (k\$)
Mechanical support&cooling (barrel)	490	-	490
Hybrid pixel layer	1410	750	660
Three silicon strip layers	2800	1270	1530
Management costs	100	-	100
Total	4800	2020	2780
Overhead on DOE contribution (~20%)	445	-	445
50% contingency	2523	910	1613
total	7768	2930	4838

<b>Construction Project 2 - EndCaps</b>	<b>DOE (k\$)</b>
<b>Mecanical support and cooling (2 endcaps)</b>	<b>195</b>
<b>Hybrid pixel layers (2 encaps)</b>	<b>4766</b>
<b>Management</b>	<b>100</b>
<b>Total</b>	<b>5061</b>
<b>Overhead on DOE contribution</b>	<b>1257</b>
<b>50% contingency</b>	<b>2458</b>
<b>Total</b>	<b>8849</b>

<sup>1</sup> R.L. Jaffe hep-ph/0201068 and references therein

<sup>2</sup> I. Sarcevic, P. Valerio, Phys. Rev C. 51, 1433 (1995)

<sup>3</sup> M. Krüger hep-ph/0106120, M. Cacciari et al., hep-ph/9803400, M. Stratmann, Eur. Phys. J. C10, 107 (1999)

<sup>4</sup> R. Vogt hep-ph/0111271

<sup>5</sup> E. Norrbin, T. Sjostrand, Eur. Phys. J. C 17, 137 (2000)

<sup>6</sup> M. Arnedo, Phys. Rep. 240, 301 (1994), K.J. Eskola et al., hep-ph/9906484

<sup>7</sup> L. Frankfurt, M. Strikman, Eur. Phys. J A5, 293 (99)

<sup>8</sup> R. Baier, D. Schiff, B.G. Zakharov, Ann. Rev. Nucl. Sci 50, 37 (2000)

<sup>9</sup> U.A. Wiedemann, Nucl. Phys. B 588, 303 (2000)

<sup>10</sup> M. Gyulassy et al., nucl-th/0006010

<sup>11</sup> kharzeev dead-cone

<sup>12</sup> E. Shuryak Phys. Rep 61, 71 (1980)

<sup>13</sup> P. Levai et al, Phys. Rev C. 51, 3326 (1995)

<sup>14</sup> Z. Lin and M. Gyulassy, Phys. Rev. C. 51, 2177 (1995)

<sup>15</sup> K. Adcox et al., Phys. Rev. Lett. 88, 19203 (2002)

<sup>16</sup> D. Kharzeev et al., Z. Phys. C. 74, 307 (1997) and references therein

<sup>17</sup> E789 Phys. Rev. Lett. 74, 3118 (1995).

<sup>18</sup> Heijne, E.H.M., Semiconductor micropattern pixel detectors: A review of the beginnings, Nucl. Instrum. Methods Phys. Res. A465 (2001) 1-26

<sup>19</sup> W.-Snoeys et al., Pixel readout electronics development for the ALICE pixel vertex and LHCb RHIC detector, Nucl. Instr. Meth. Phys. Res. A465 (2001) 176--189

<sup>20</sup> The ALICE Collaboration, ALICE - Technical Design Report of the Inner Tracking System, CERN/LHCC 99-12, 18 June 1999

<sup>21</sup> <http://ssd-rd.web.cern.ch/ssd-rd/rd/talks/Li-rd-2001.pdf>

<sup>22</sup> svx4 reference

<sup>23</sup> HYTEC report